Journal of Physics D: Applied Physics

PAPER

Exploring new phases of $Fe_{3-x}Co_xC$ for rare-earth-free magnets

To cite this article: S Q Wu *et al* 2017 *J. Phys. D: Appl. Phys.* **50** 215005

IOP Publishing Journal of Physics D: Applied Physics
J. Phys. D: Appl. Phys. **50** (2017) 215005 (7pp) https://doi.org/10.1088/1361-6463/aa6b85

Exploring new phases of $Fe_{3-x}Co_xC$ for rare-earth-free magnets

S Q Wu[1,2], B Balamurugan[3], X Zhao[1], S Yu[1,2], Manh Cuong Nguyen[1], Y Sun[1], S R Valloppilly[3], D J Sellmyer[3], K M Ho[1] and C Z Wang[1]

[1] Ames Laboratory, US DOE and Iowa State University, Ames, IA 50011, United States of America
[2] Department of Physics, Collaborative Innovation Center for Optoelectronic Semiconductors and Efficient Devices, Xiamen University, Xiamen 361005, People's Republic of China
[3] Nebraska Center for Materials and Nanoscience and Department of Physics and Astronomy, University of Nebraska, Lincoln, NE 68588, United States of America

E-mail: wangcz@ameslab.gov

Received 31 January 2017, revised 27 March 2017
Accepted for publication 5 April 2017
Published 9 May 2017

Abstract

Structures, magnetic moments, and magnetocrystalline anisotropy energies of the $Fe_{3-x}Co_xC$ intermetallic compounds are systematically investigated using adaptive genetic algorithm (AGA) crystal-structure predictions and first-principles calculations. Besides reproducing the known cementite (*Pnma*) structure of Fe_3C, i.e. $x = 0$, the AGA searches also capture several new metastable phases within the room-temperature range. In particular, a bainite ($P6_322$) structure exhibits the largest magnetic moment among all low-energy structures, and its energy is only 4 meV/atom higher than the cementite (*Pnma*) phase. The atomic structure of the *Pnma* Fe_2CoC phase, i.e. $x = 1$, is also identified, and the calculated x-ray diffraction spectrum, magnetocrystalline anisotropy energy, and saturation magnetization based on the structure from our theoretical study are in good agreement with experiment.

Keywords: structure prediction, magnetic properties, rare-earth free, first-principles calculation

(Some figures may appear in colour only in the online journal)

1. Introduction

Fe–Co alloys have been continuously attracting intensive studies due to their potential applications in magnetic devices. In particular, these alloys occupy a prominent position in the search for rare-earth-free permanent magnets because of their high intrinsic magnetic moment [1]. However, the cubic symmetry of the alloys produces negligible magnetocrystalline anisotropy energy (MAE), which is unsuitable for permanent magnets. To overcome this problem, considerable effort has been devoted to stabilize non-cubic crystalline structures in these alloys by non-equilibrium synthesis methods or by adding a third element [2–11]. It was first proposed that through straining the unit cell (i.e. changing the *c*/*a* ratio), remarkably high MAEs could be achieved [1]. Yet up to now, tetragonal distorted Fe–Co alloys can be produced only for thin films with very few monolayers. Alternatively, doping lighter elements such as B, C, or N into the Fe–Co alloys also has been explored to achieve either the stabilization of the tetragonal distortion [1–5, 10] or the formation of new crystal phases that possess high intrinsic MAE [7–9]. In this work, we report our study on the structures and magnetic properties of carbon-alloyed Fe–Co, specifically on the compositions of $Fe_{3-x}Co_xC$ ($0 \leqslant x \leqslant 3$).

Recently, Choe *et al* [10] investigated the magnetic properties of the electrolytically extracted cementite Fe_3C (S.G. *Pnma*) phase and found its easy axis of magnetization is the *c*-axis, but this material exhibits only a moderate MAE of about 4 Mergs cm^{-3} at 5 K. However, it was reported a high blocking temperature, $T_B = 790$ K, for $CoFe_2C$ nanoparticles, indicating a significantly improved magnetic anisotropy in the $CoFe_2C$ phase [7]. Cobalt carbide nanoparticles also have shown appreciable permanent-magnetic properties [12], but these nanoparticles are composed of Co_3C having cementite (*Pnma*) structure along with Co_2C phase [12, 13]. It is worth noting that crystalline phases prepared by thin-film and nanoparticle synthesis techniques also can be formed with non-equilibrium fabrication methods [14]. In addition,

these methods increase the prospect to obtain new phases/structures, which may exhibit desirable magnetic properties. In this regard, a comprehensive knowledge about not only the ground state but also various metastable crystalline structures in a given chemical composition would be very useful for guiding experimental investigations in the design and discovery of novel magnetic materials.

Using adaptive genetic algorithm (AGA) and first-principles calculations, $Fe_{3-x}Co_xC$ $(0 \leqslant x \leqslant 3)$ is studied systematically in this work. Several new metastable phases which can be stable within the room-temperature range are captured. In addition, a bainite ($P6_322$) structure exhibits the largest magnetic moment among all the low-energy structures from our AGA search, and its energy is only 4 meV/atom higher than the cementite (*Pnma*) phase. The atomic structures and MAEs of the *Pnma* phase for Fe_2CoC are also determined and a good agreement is found between our experiments and theoretical calculations.

2. Methods

In this paper, the low-energy structures of binary and ternary $Fe_{3-x}Co_xC$ $(0 \leqslant x \leqslant 3)$ material systems were determined by global search using the AGA method [15]. In the AGA method, the configuration space of the crystal structures is explored by fast genetic algorithm searches using auxiliary classical potentials. The auxiliary classical potential is updated on-the-fly in an iterative process where the parameters of the classical potentials are adjusted by comparing the results of the energies, forces and stresses of the structures from the classical potentials with those of the DFT calculations. The potential fitting is performed using a force-matching method with the stochastic simulated annealing algorithm as implemented in the POTFIT code [16, 17]. In this study, classical potentials in the form based on the embedded-atom method (EAM) are used. The DFT calculations were performed using the Vienna *ab initio* simulation package (VASP) [18, 19], which is based on the spin-polarized density-functional theory, the plane-wave basis and the projector augmented wave (PAW) representation. The exchange-correlation functional is treated within the generalized-gradient approximation (GGA), in the form of Perdew–Burke–Ernzerhof (PBE) [20]. A 400 eV kinetic-energy cutoff was chosen for the plane-wave basis set, and Brillouin-zone integrations were carried out using the Monkhorst–Pack scheme [21] with *k*-point mesh resolution of $2\pi \times 0.03$ Å^{-1}.

3. Results and discussion

3.1. Binary Fe_3C and Co_3C

Crystal structures of Fe_3C binary alloy with unit cells containing up to 4 formula units (f.u.) are searched using our AGA method. The energy *versus* volume for the low-energy structures obtained from our AGA search is shown in figure 1(a). Both θ-Fe_3C (cementite) and ε-Fe_3C (bainite) phases are found in our optimized structure pool. The orthorhombic

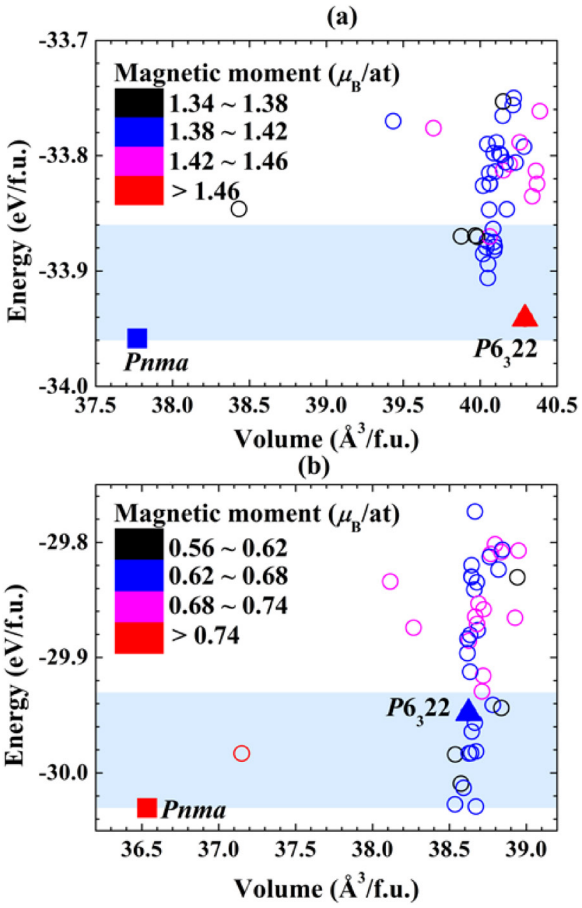

Figure 1. Energy versus volume for the low-energy structures of (a) Fe_3C and (b) Co_3C obtained from the AGA searches. The θ (*Pnma*) and ε ($P6_322$) phases are highlighted with the square and triangle, respectively. The colors used for the symbols are related to the magnitude of the magnetic moment of each structure as indicated by the color bar in the figure.

θ-Fe_3C (S.G. *Pnma*, $Z = 4$) is found to be the lowest-energy structures for Fe_3C system, while ε-Fe_3C ($P6_322$) is a metastable one with its energy only around 4 meV/atom higher compared to θ-Fe_3C phase. We note that the volume of the ε-Fe_3C ($P6_322$) phase (40.29 Å^3/f.u.) is much larger than that of the θ-Fe_3C (*Pnma*) phase (37.77 Å^3/f.u.). It is also interesting to note that almost all the low-energy structures obtained from the AGA search have a volume similar to that of the ε-Fe_3C ($P6_322$) phase.

We found that most of the low-energy structures obtained from our AGA search can be viewed as Fe layers derived from a hexagonal close packed (HCP) structure, with C atoms occupying interstitial sites. As shown in figure 2(a), the Fe atoms in the structure of θ-Fe_3C arrange in pleated layers, which is much distorted from the HCP structure. The calculated lattice constants (5.027, 6.713, 4.477 Å) match well with the experimental values (5.0825(2), 6.733(1), 4.5119(3) Å) [22] and the previous calculated results (5.0368, 6.7203, 4.4818 Å) [23], (5.058, 6.703, 4.506 Å) [24]. ε-Fe_3C crystallizes in the hexagonal space group $P6_322$ (S.G. # 182) with two formula units ($Z = 2$) per unit cell, where six Fe atoms and two carbon atoms are in the interstices as shown in figure 2(b) [25, 26]. Besides the two phases mentioned above, more than 10

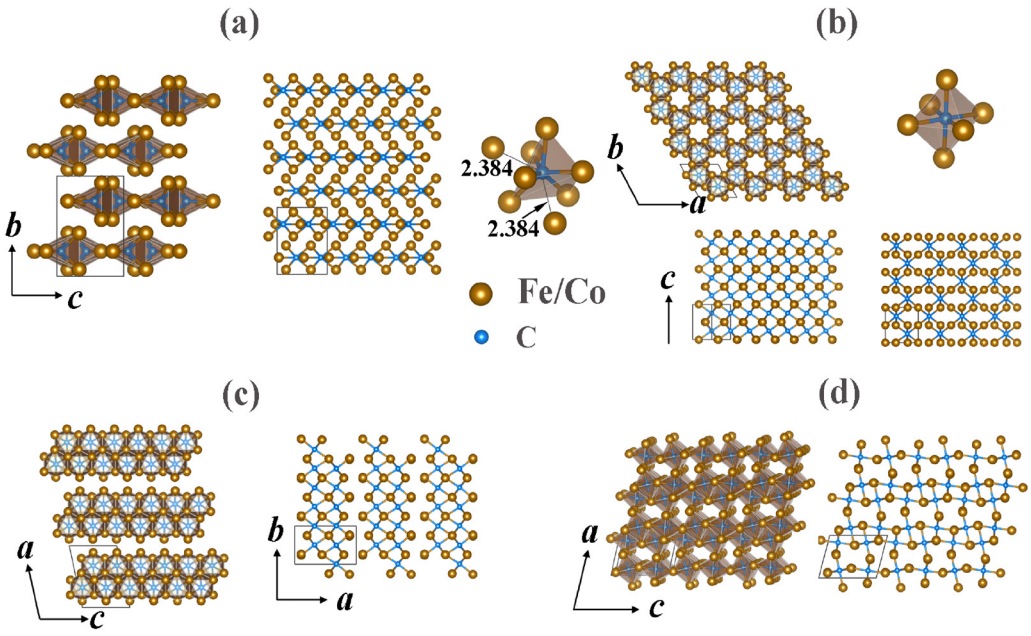

Figure 2. Some typical low-energy structures of Fe_3C and Co_3C. (a) *Pnma* (type 1), (b) $P6_322$ (type 2), (c) $P2_1/c$ (type 3), P-1 (type 4).

metastable phases are found in the room-temperature window (the light-blue shaded region) from the ground-state *Pnma* structure as shown in figure 1(a).

As one can see from figure 1, the low-energy structures of Fe_3C and Co_3C obtained from our AGA search are clearly divided into a small volume group and a larger volume group. These low-energy structures can be further classified into four types of structures as shown in figure 2, where one typical structure of each type is shown. Type 1 structures locate in the small-volume region, i.e. with higher atomic density, while all the other three types belong to the large-volume group. The coordination of C atoms in Type 1 structures is CFe_{6+2}, i.e. six nearest Fe atoms form a triangular prism with a C atom in the center, while the other two Fe atoms form relatively larger C–Fe bonds with the centered C atom as shown in figure 2(a). In all the other three type structures, Fe atoms form HCP AB stacking layers with C atoms occupy different interstitial sites of the HCP lattice and result in different structure types (Type 2, 3 & 4). In Type 2 structure, the distribution of C atoms is more uniform which leads to relatively high-symmetry structure. Type 3 structures can be considered as 'layered' structures, while the Fe lattice of Type 4 structure is more distorted due to inhomogeneous distribution of C atoms. Although the Type 1 *Pnma* structure is the lowest-energy structure, majority of the low-energy structures belong to Type 2 and Type 3. If we plot the energies of these 4 structural types using different colors as shown in figure 3, we can see that the Type 2 structures are energetically more favorable for the Fe_3C structures than for the Co_3C structures, while the opposite is true for the Type 3 structures.

The magnetic moments of the different Fe_3C and Co_3C structures are shown in figure 1 and table 1. Bainite Fe_3C (S.G. $P6_322$) exhibits the largest magnetic moment (1.48 μ_B/at) among all the structures in the Fe_3C pool, yet its energy is only 4 meV/atom higher than the cementite (*Pnma*) phase, which has a lower magnetic moment (1.38 μ_B/at). In the

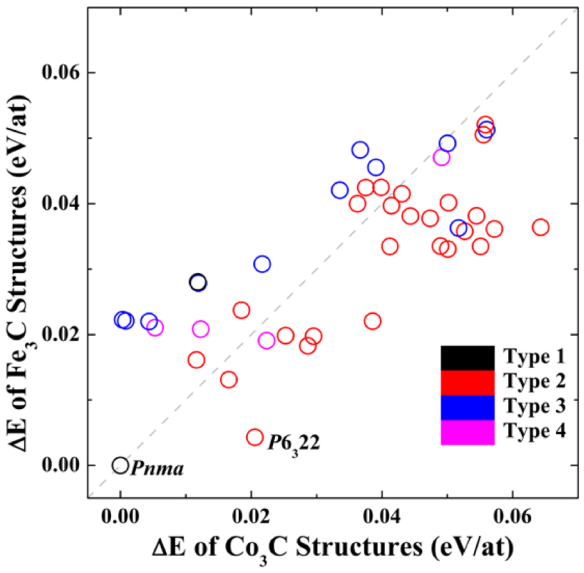

Figure 3. Correlation between the relative energies of Fe_3C and Co_3C structures. The energies of *Pnma* Fe_3C and *Pnma* Co_3C are taken as references, respectively.

Co_3C system, the most stable phase, i.e. cementite, exhibits the largest magnetic moment (0.78 μ_B/at) and also the largest MAE of 8.1 Mergs cm^{-3} among all the Co_3C structures in the pool. The calculated MAE for *Pnma* Fe_3C is relatively small (0.5 Mergs cm^{-3}), which is smaller than the experimental value [10]. The largest MAE among all the Fe_3C structures in the pool is for the *Pm* phase with a value of 12.4 Mergs cm^{-3}.

3.2. Ternary $Fe_{3-x}Co_xC$

As shown above, Fe_3C and Co_3C compounds exhibit different magnetic properties, including magnetic moments and MAEs, even for the counterparts with the same crystal structure. It is interesting to investigate the structures and magnetic

Table 1. Structural and magnetic properties of Fe_3C and Co_3C.

	Space group (SG)	SG #	Moment μ_B/at	Theo. MAE (μeV/at)	Theo. MAE (Mergs cm^{-3})	Expt. MAE (Mergs cm^{-3})	Structure type
Fe_3C (cementite)	Pnma	62	1.38	3	0.5	4.05[a]	Type 1
Fe_3C (bainite)	$P6_322$	182	1.48	36	5.7		Type 2
Fe_3C	*Pm*	6	1.43	78	12.4		Type 4
Co_3C	*Pnma*	62	0.78	46	8.1		Type 1
Co_3C	$P6_322$	182	0.69	1	0.2		Type 2
Co_3C	$P2_1/c$	14	0.65	40	7.0		Type 3

[a]Ref. [10].

properties of M_3C compounds with mixed Fe/Co ratios in the M sites. We therefore studied ternary $Fe_{3-x}Co_xC$ using the AGA method (for $x = 1$) and by substitution (for $x = 0.5$, 1.0, 1.5, 2.0, 2.5) based on the several low-energy structures found in the binary systems. A convex hull of formation energies relative to the *Pnma* Co_3C and *Pnma* Fe_3C phases for ternary $Fe_{3-x}Co_xC$ is given in figure 4. Both AGA and substitution methods found many structures in the ternary system with negative formation energies.

The magnetic moment and MAE of the lowest-energy structure for each ternary $Fe_{3-x}Co_xC$ composition are shown in table 2. Among all these structures, the ones with x equal to 1.0, 2.0 and 2.5 are stable against phase decomposition as shown in figure 4. The MAEs for these five structures are all quite small. We also list some structures with relatively high MAEs in table 3. The relative energies of these structures are only about 7 meV/atom to 42 meV/atom higher than that of the corresponding lowest-energy structure at the same composition. Therefore, these metastable structures might be synthesized at high temperature or by non-equilibrium synthesis methods.

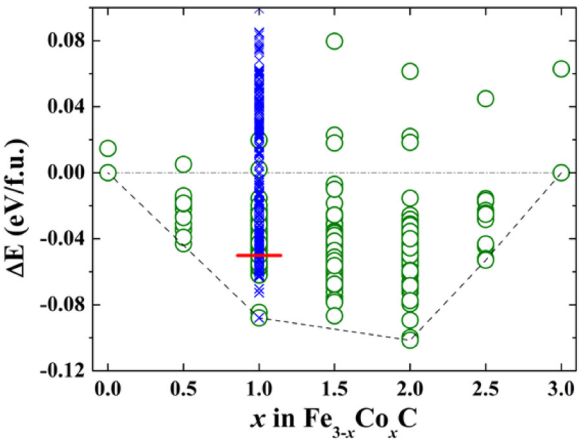

Figure 4. Convex hull of formation energies in ternary $Fe_{3-x}Co_xC$. The formation energy is defined relative to the *Pnma* Co_3C and *Pnma* Fe_3C phases. Red horizontal line shows the energy of *Pnma* Fe_2CoC whose simulated XRD pattern matches well with the experimental one.

3.3. Fe_2CoC

We have fabricated Fe_2CoC alloys using a conventional arc-melting method followed by a melt-spinning process. High purity elements such as Fe, Co and C were arc-melted to form a homogeneous alloy with Fe_2CoC composition, which was subsequently made into nanocrystalline ribbons via rapid quenching from the melt using the melt-spinning process. For x equal to 1.0, i.e. Fe_2CoC, a structure with the *Pnma* space group is found in our AGA pool. Interestingly, the simulated XRD pattern based on the atomic structure of Fe_2CoC from our theoretical study is in very good agreement with the measured experimental XRD pattern for the melt-spun Fe_2CoC alloy as shown in figure 5.

The relative intensity of the peak at ~53º in the experimental XRD pattern suggests the existence of another phase, possibly BCC Fe. The comparison in firgure 5 indicates that BCC Fe could be the minority phase in the experimental sample which contributes to the high intensity of the peak at ~53°, although the peak position of simulated XRD pattern of BCC Fe is a little bit larger compared to the experiment one. Besides, the fully relaxed *Pnma* structure shows a double peak at ~53°, corresponding to (2 2 0) and (0 3 1) faces respectively, compared to the 'merged' single peak from experiment. In order to estimate the amount of Fe, we have carried out the Rietveld analysis of the experimental XRD pattern as shown in figure 6(a). Note that melt-spun ribbons often exhibit texture effects [27, 28], and thus a minor (0 0 1) and (1 1 0) texturing was introduced to obtain a better fitting in figure 6(a). This analysis shows a presence of about 90 wt.% Fe_2CoC phase and 10 wt.% BCC Fe in the experimental sample.

We also have measured the magnetic properties of the melt-spun Fe_2CoC alloys using a superconducting quantum interference device (SQUID) magnetometer. Figure 6(b) shows the field-dependent magnetization curves measured at 300 K and 10 K. We have applied the law-approach-to-saturation (LAS) method to estimate the magnetocrystalline anisotropy consatnt K_1 and saturation magnetization M_s [29]. In this method, the high-field magnetization curves between 20 and 70 kOe were fitted using the equation $M = M_s(1-4K_1^2/15M_s^2H^2) + \chi$H as shown in figure 6(c), where χ is the high-field magnetic susceptibility [29]. This analysis yields $K_1 = 10$ Mergs cm^{-3} and $M_s = 1190$ emu cm^{-3} ($\approx$1.23 μ_B/atom) at 10 K and $K_1 = 9.1$ Mergs cm^{-3} and $M_s = 1122$ emu cm^{-3} ($\approx$1.16 μ_B/atom) at 300 K.

Note that the experimental sample has only a minor Fe fraction of about 10 wt.% ($\approx$9.9 vol.% Fe). However, the expanded hysteresis loop measured at 10 K, shown in figure 6(d), indicates a single-phase behavior and suggests a strong exchange coupling between the Fe and Fe_2CoC phases.

Table 2. Magnetic moments and magnetocrystalline anisotropy energies (MAEs) of lowest-energy ternary $Fe_{3-x}Co_xC$ phases.

System	Space group (SG)	SG #	ΔE (meV/f.u.)	Moment (μ_B/at)	Theo. MAE (μeV/at)	Theo. MAE (Mergs cm^{-3})
$Fe_{2.5}Co_{0.5}C$	$P2_1$	4	−0.043	1.29	15	2.6
Fe_2CoC	$P2_1/c$	14	−0.088	1.23	9	1.5
$Fe_{1.5}Co_{1.5}C$	$P2_1$	4	−0.087	1.11	5	0.9
$FeCo_2C$	$Pna2_1$	33	−0.102	0.96	15	2.6
$Fe_{0.5}Co_{2.5}C$	$P2_1$	4	−0.053	0.89	19	3.3

Table 3. Magnetic properties of ternary $Fe_{3-x}Co_xC$ phases with relatively higher MAEs.

System	Space group (SG)	SG #	ΔE (meV/f.u.)	Moment μ_B/at	Theo. MAE (μeV/at)	Theo. MAE (Mergs cm^{-3})	Expt. MAE (Mergs cm^{-3})
$Fe_{2.5}Co_{0.5}C$	$C2$	5	−0.015	1.38	56	9.0	
Fe_2CoC	$Pnma$	62	−0.050	1.18	38	6.5	9.6
Fe_2CoC	$C2$	5	0.022	1.29	46	7.4	
$Fe_{1.5}Co_{1.5}C$	$P321$	150	0.080	1.15	85	13.7	
$Fe_{1.5}Co_{1.5}C$	Pm	6	0.023	1.11	32	5.5	
$FeCo_2C$	$P1$	1	−0.060	1.00	40	6.9	

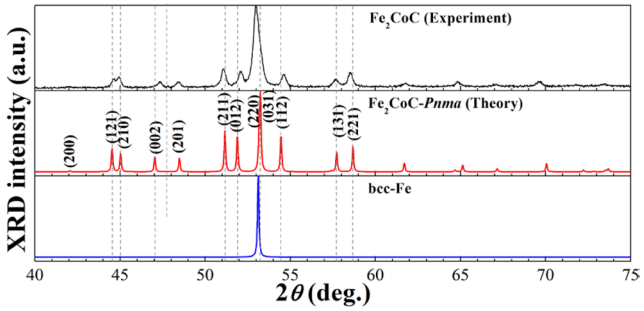

Figure 5. Simulated and experimental XRD patterns. Gray dashed lines indicate the peak positions of *Pnma* phase with experimental lattice constants.

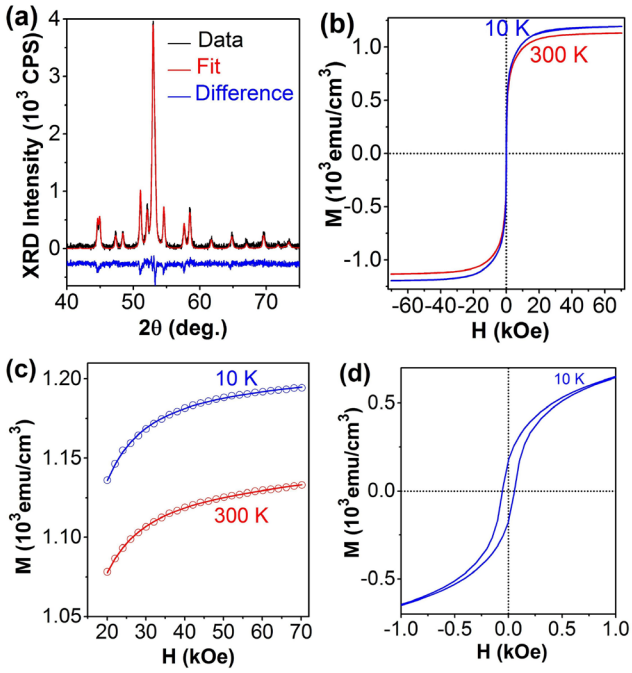

Figure 6. Fe_2CoC alloys: (a) experimental XRD pattern and the Rietveld fit. The curve at the bottom is the difference between the measured pattern and the fit. (b) Hysteresis loops measured at 300 K and 10 K. (c) An estimation of magnetic anisotropy constant K_1 and saturation magnetization M_s from the high-field region of the magnetization curves using the law of approach to saturation method. The open spheres and lines represent the corresponding experimental data and fitting, respectively. (d) The expanded hysteresis loop measured at 10 K.

For a two-phase exchange-coupled nanocomposite system, the resultant magnetization can be generally written as f_hM_s (hard) + f_sM_s (soft). f_h and M_h (hard) and f_s and M_s (soft) are the volume fractions and saturation magnetizations of the hard and soft phases, respectively. By using the equation for the resultant magnetization, experimental M_s values determined from the LAS analysis for the melt-spun alloy having Fe_2CoC and Fe phases, and standard M_s value for Fe (about 1710 emu cm^{-3}) [30], we calculated the M_s values for the individual Fe_2CoC phase in the ribbon sample as about 1133 emu cm^{-3} (≈1.17 μ_B/atom) at 10 K and 1057 emu cm^{-3} (≈1.09 μ_B/atom) at 300 K. Similarly, we also estimated the anisotropy constant of the Fe_2CoC phase by taking into account of the minority Fe phase in the melt-spun alloy. Since Fe has a very low anisotropy field (0.6 kOe) [30], the slope of the high-field magnetization curves used for LAS analysis in figure 6(c) mainly originates from the magnetic anisotropy of the hard Fe_2CoC phase, in addition to the high-field magnetic susceptibility. Thus, by considering only the individual magnetization of the Fe_2CoC phase in the melt-spun alloy, K_1 for Fe_2CoC is semiquantitatively estimated as about 9.6 Mergs cm^{-3} at 10 K and about 8.6 Mergs cm^{-3} at 300 K.

The experimental magnetic moments obtained for Fe_2CoC are in very good agreement with the theoretical value (1.18 μ_B/atom). Although the theoretical MAE value (6.5 Mergs cm^{-3}), as shown in table 3, is somewhat lower than the experimental one for the Fe_2CoC phase (9.6 Mergs cm^{-3}), the atomic structure matches very well with the experimental one. Previously,

Table 4. Structural parameters of *Pnma* Fe_2CoC.

Fe_2CoC		Theo.	Expt.
Space group		*Pnma*	
(*a*, *b*, *c*) (Å)		(5.0245, 6.7084, 4.4676)	(5.055, 6.756, 4.505)
Fe	8*d*	(0.1787, 0.5692, 0.8327)	
Co	4*c*	(−0.0354, 0.2500, 0.6568)	
C	4*c*	(0.1256, 0.2500, 0.0494)	

Qian *et al* [31] have also reported the magnetic properties of *Pnma* Fe_2CoC material, and given relatively larger atomic magnetic moment and the MAE comparing with those from our experiments, which could be due to the GGA + U approach used in their work. In addition, our predicted structural parameters together with the experimental lattice parameters of *Pnma* Fe_2CoC are presented in table 4.

4. Conclusions

In conclusion, stable and metastable structures, and magnetic properties for binary and ternary (Fe, $Co)_3C$ systems have been studied by combining the AGA method with density-functional theory calculations and experimental synthesis and characterization. The detailed structural properties of M_3C systems have been analyzed. Besides reproducing the known cementite (*Pnma*) structure of Fe_3C, the AGA searches also capture several new metastable phases within the room-temperature range. In particular, a bainite ($P6_322$) structure exhibits the largest magnetic moment among all the structures in the Fe_3C pool, yet its energy is only 4 meV/atom higher than that of the cementite (*Pnma*) phase. The relative stabilities among the structures for Co_3C are quite different from those for Fe_3C system, but the cementite is still the ground-state phase. Cementite Co_3C exhibits the largest magnetic moment (0.78 μ_B/at) and also the largest magnetocrystalline anisotropy energy among all the Co_3C structures. We also identify the atomic structures of the *Pnma* phase for Fe_2CoC. The experimental x-ray spectrum for Fe_2CoC can be understood by combining the *Pnma* Fe_2CoC that found in our AGA search with a minor BCC Fe phase.

Acknowledgments

Theoretical study was supported by the National Science Foundation (NSF), Division of Materials Research (DMR) under Award DMREF: SusChEM 1436386. Experimental work was supported by NSF, DMR, under Award DMREF: SusChEM 1436385. The development of adaptive genetic algorithm (AGA) method was also supported by the US Department of Energy, Basic Energy Sciences, Division of Materials Science and Engineering, under Contract No. DE-AC02-07CH11358, including a grant of computer time at the National Energy Research Scientific Computing Center (NERSC) in Berkeley, CA. Research at Nebraska was performed in part in the Nebraska Nanoscale Facility, Nebraska Center for Materials and Nanoscience, which is supported by the NSF under Award NNCI: 1542182, and the Nebraska Research Initiative (NRI). Authors acknowledge Bhaskar Das for his assistance in the preparation of melt-spun ribbons.

References

[1] Burkert T, Nordstrom L, Erikson O and Heinonen O 2004 Giant magnetic anisotropy in tetragonal FeCo alloys *Phys. Rev. Lett.* **93** 027203
[2] Al-Zoubi N, Skorodumova N V, Medvedeva A, Andersson J, Nilson G, Johansson B and Vitos L 2012 Tetragonality of carbon-doped ferromagnetic iron alloys: a first-principles study *Phys. Rev.* B **85** 014112
[3] Delczeg-Czirjak E K, Edstrom A, Werwinski M, Rusz J, Skorodumova N V, Vitos L and Eriksson O 2014 Stabilization of the tetragonal distortion of Fe_xCo_{1-x} alloys by C impurities: a potential new permanent manget *Phys. Rev.* B **89** 144403
[4] Reichel L, Schultz L and Fahler S 2015 Lattice relaxation studies in strained epitaxial Fe–Co–C films *J. Appl. Phys.* **117** 17C712
[5] Khan I and Hong J 2015 Magnetic anisotropy of C and N doped bulk FeCo alloy: a first principles study *J. Magn. Magn. Mater.* **388** 101–5
[6] Lv Z Q, Zhang F C, Sun S H, Wang Z H, Jiang P, Zhang W H and Fu W T 2008 First-principles study on the mechanical, electronic and magnetic properties of Fe_3C *Comput. Mater. Sci.* **44** 690–4
[7] El-Gendy A A, Bertino M, Clifford D, Qian M, Khanna S N and Carpenter E E 2015 Experimental evidence for the formation of $CoFe_2C$ phase with colossal magnetocrystalline-anisotropy *Appl. Phys. Lett.* **106** 213109
[8] Zhao X, Ke L, Wang C Z and Ho K M 2016 Metastable cobalt nitride structures with high magnetic anisotropy of rare-earth free magnets *Phys. Chem. Chem. Phys.* **18** 31680–90
[9] Zhao X, Wang C Z, Yao Y and Ho K M 2016 Large magnetic anisotropy predicted for rare-earth free $Fe_{16-x}Co_xN_2$ alloys *Phys. Rev.* B **94** 224424
[10] Choe H, Terai T, Fukuda T, Kakeshita T, Yamamoto S and Yonemura M 2016 Easy axis of magnetization of Fe_3C prepared by an electrolytic extraction method *J. Magn. Magn. Mater.* **417** 1–5
[11] Pal S K, Skokov K P, Groeb T, Ener S and Gutfleisch O 2017 Properites of magnetically se-hard $(Fe_xCo_{1-x})_3B$ compounds *J. Alloys Compd.* **696** 543
[12] Harris V G *et al* 2010 High coercivity cobalt carbide nanoparticles processed via polyol reaction: a new permanent magnet material *J. Phys. D: Appl. Phys.* **43** 165003
[13] Syugaev A V, Lyalina N V, Lomayeva S F and Maratkanova A N 2015 Electrochemical behavior of Co_3C carbide *J. Solid State Electrochem.* **19** 2933
[14] Balamurugan B, Das B, Zhang W Y, Skomski R and Sellmyer D J 2014 Hf–Co and Zr–Co alloys for rare-earth-free permanent magnets *J. Phys.: Condens. Matter* **26** 064204
[15] Wu S Q, Ji M, Wang C Z, Nguyen M C, Zhao X, Umemoto K, Wentzcovitch R M and Ho K M 2014 An adaptive genetic algorithm for crystal structure prediction *J. Phys.: Condens. Matter* **26** 035402
[16] Brommer P and Gähler F 2006 Effective potentials for quasicrystals from *ab initio* data *Phil. Mag.* **86** 753
[17] Brommer P and Gähler F 2007 Potfit: effective potentials from *ab initio* data *Model. Simul. Mater. Sci. Eng.* **15** 295–304
[18] Kresse G and Furthmüller J 1996 Efficient iterative schemes for *ab initio* total-energy calculations using a plane-wave basis set *Phys. Rev.* B **54** 11169–86
[19] Kresse G and Furthmüller J 1996 Efficiency of *ab initio* total energy calculations for metals and semiconductors using a plane-wave basis set *Comput. Mater. Sci.* **6** 15–50

[20] Perdew J P, Burke K and Ernzerhof M 1996 Generalized gradient approximation made simple *Phys. Rev. Lett.* **77** 3865–8
[21] Monkhorst H J and Pack J D 1976 Special points for Brillouin-zone integrations *Phys. Rev.* B **13** 5188–92
[22] Wood I G, Vočadlo L, Knight K S, Dobson D P, Marshall W G, Price G D and Brodholt J 2004 Thermal expansion and crystal structure of cementite, Fe_3C, between 4 and 600 K determined by time-of-flight neutron powder diffraction *J. Appl. Crystallogr.* **37** 82
[23] Fang C M, van Huis M A and Zandbergen H W 2009 Structural, electronic, and magnetic properties of iron carbide Fe_7C_3 phases from first-principles theory *Phys. Rev.* B **80** 224108
[24] Shein I R, Medvedeva N I and Ivanovskii A L 2006 Electronic and structural properties of cementite-type M_3X (M = Fe, Co, Ni; X = C or B) by first principles calculations *Physica* B **371** 126
[25] Yakel H L 1985 Crystal structures of stable and metastable iron-containing carbides *Int. Met. Rev.* **30** 17
[26] Jacobs H, Rechenbach D and Zachwieja U 1995 Structure determination of γ'-Fe_4N and ϵ-Fe_3N *J. Alloys Compd.* **227** 10
[27] Nelson A, Kharel P, Huh Y, Fuglsby R, Guenther J, Zhang W, Staten B, Lukashev P, Valloppilly S and Sellmyer D J 2015 Enhancement of Curie temperature in Mn_2RuSn by Co substitution *J. Appl. Phys.* **117** 153906
[28] Zaluzka A, Xu Y, Altounian Z and Strom-Olsen J O 1991 Effects of quench rate on the texture in melt-spun Nd–Fe–B alloys *Mater. Sci. Eng.* A **133** 819
[29] Hadjipanayis G C, Sellmyer D J and Brandt B 1981 Rare-earth-rich metallic glasses. I. Magnetic hysteresis *Phys. Rev.* B **23** 3349
[30] Skomski R 2003 Nanomagnetics *J. Phys.: Condens. Matter* **15** R841
[31] Qian M and Khanna S N 2013 Magnetic properties of $Co_{2-x}TM_xC$ and $Co_{3-x}TM_xC$ nanoparticles *J. Appl. Phys.* **114** 243909